

Environments around quasars at $z \sim 3$ revealed by wide-field imaging with Subaru HSC and CFHT

YUTA SUZUKI ¹, HISAKAZU UCHIYAMA ^{2,3}, YOSHIKI MATSUOKA ³, JUN TOSHIKAWA ^{4,5}, STEPHEN GWYN ⁶,
MASATOSHI IMANISHI ^{2,7,8}, CHENGZE LIU ⁹, AKATOKI NOBORIGUCHI ¹⁰, MARCIN SAWICKI ¹¹ AND
YOSHIKI TOBA ^{2,3,12}

¹Graduate School of Science and Engineering, Ehime University, 2-5 Bunkyo-cho, Matsuyama, Ehime 790-8577, Japan;
yuta@cosmos.phys.sci.ehime-u.ac.jp

²National Astronomical Observatory of Japan, 2-21-1 Osawa, Mitaka, Tokyo 181-8588, Japan

³Research Center for Space and Cosmic Evolution, Ehime University, 2-5 Bunkyo-cho, Matsuyama, Ehime 790-8577, Japan

⁴Nishi-Harima Astronomical Observatory, Center for Astronomy, University of Hyogo, Sayo, Hyogo 679-5313, Japan

⁵Department of Physics, University of Bath, Claverton Down, Bath, BA2 7AY, UK

⁶NRC-Herzberg, 5071 West Saanich Road, Victoria, British Columbia V9E 2E7, Canada

⁷Department of Astronomy, School of Science, Graduate University for Advanced Studies (SOKENDAI), Mitaka, Tokyo 181-8588, Japan

⁸Toyo University, 5-28-20, Hakusan, Bunkyo-ku, Tokyo 112-8606, Japan

⁹Department of Astronomy, School of Physics and Astronomy, and Shanghai Key Laboratory for Particle Physics and Cosmology, Shanghai Jiao Tong University, Shanghai 200240, People's Republic of China

¹⁰Center for General Education, Shinshu University, 3-1-1 Asahi, Matsumoto, Nagano 390-8621, Japan

¹¹Institute for Computational Astrophysics and Department of Astronomy and Physics, Saint Mary's University, 923 Robie Street, Halifax, Nova Scotia, B3H 3C3, Canada

¹²Academia Sinica Institute of Astronomy and Astrophysics, 11F of Astronomy-Mathematics Building, AS/NTU, No.1, Section 4, Roosevelt Road, Taipei 10617, Taiwan

ABSTRACT

We examine the local density environments around 67 quasars at $z \sim 3$, by combining the imaging data of Hyper Suprime-Cam Subaru Strategic Program (HSC-SSP) and Canada-France-Hawaii Telescope Large Area U-band Survey (CLAUDS) over about 20 deg². Our measurements exploit U -dropout galaxies in the vicinities of quasars taken from Sloan Digital Sky Survey (SDSS). We find that the quasars have the indistinguishable surrounding density distribution from the U -dropout galaxies, and that three quasars are associated with protocluster candidates within a projected separation of 3 arcmin. According to a halo evolutionary model, our results suggest that quasars at this epoch occupy haloes with a typical mass of $1.3^{+1.4}_{-0.9} \times 10^{13} h^{-1} M_{\odot}$. We also investigate the dependence of the local galaxy overdensity on ultraviolet (UV) luminosities, black hole (BH) masses, and proximity zone sizes of the quasars, but no statistically-significant correlation was found. Finally, we find that the local density of faint U -dropout galaxies are lower than that of bright U -dropout galaxies within a projected distance of 0.51 ± 0.05 physical Mpc, where the quasar UV radiation is 30 times intenser than background UV radiation. We argue that photoevaporation may suppress galaxy formation at short distances where the quasar UV intensity is strong, even in massive haloes.

1. INTRODUCTION

Quasars are one of the most luminous objects in the Universe. The strong ultraviolet (UV) radiation from quasars is expected to ionize gas and suppress star formation in not only the host but also the surrounding haloes (“photoevaporation”; Benson et al. 2002; Kashikawa et al. 2007; Utsumi et al. 2010; Simpson et al. 2014; Kikuta et al. 2017; Uchiyama et al. 2019). In order to fully understand galaxy formation and evolution, we thus need to characterize where quasars appear in the large scale structure of galaxies, both observationally and theoretically.

Clustering analysis is a good approach to measure the average halo environments of quasars. At $z < 3$, quasars are found to reside in the same environments as do galaxies, with the quasar minimum dark matter (DM) halo masses estimated to be $\sim 10^{11.5-12} h^{-1} M_{\odot}$ (Myers et al. 2006; Ross et al. 2009; White et al. 2012; Font-Ribera et al. 2013). These DM halo masses are not the most massive haloes nor the progenitors of the most massive local clusters at $z < 3$ (e.g., Fanidakis et al. 2013).

At $z \sim 3$ and beyond, quasar environments are still unclear. Shen et al. (2007) found a significantly larger minimum DM halo mass of $(2 - 3) \times 10^{12} h^{-1} M_{\odot}$ for

quasars taken from Sloan Digital Sky Survey (SDSS: York et al. 2000). It indicates that a significant fraction of the quasar haloes at $z \sim 3$ evolve into present-day massive galaxy clusters. On the other hand, Eftekharzadeh et al. (2015) used the data from Baryon Oscillation Spectroscopic Survey (BOSS: Dawson et al. 2013) and found a minimum DM halo mass of $(0.60 - 0.72) \times 10^{12} h^{-1} M_{\odot}$ for quasars at $z \sim 3$, which is comparable to those found at $z < 3$. The discrepancy between the halo mass measurements by Shen et al. (2007) and Eftekharzadeh et al. (2015) remains controversial.

Another method to quantify the environments is to measure galaxy number density around quasars. Falder et al. (2011) investigated the environments of 46 luminous quasars ($M_i \lesssim -26$) at $0.3 < z < 5.3$ using Spitzer Space Telescope/Infrared Array Camera (IRAC: Fazio et al. 2004). 11 quasars at $z \sim 3$ were found to live in $\sim 2\sigma$ overdense regions on average. Fossati et al. (2021) examined 27 quasar environments by using Very Large Telescope (VLT)/Multi Unit Spectroscopic Explorer (MUSE: Bacon et al. 2010). They found that the number density of Ly α Emitters (LAEs) around quasars is higher at 3.6σ significance than in blank fields. However, the galaxy sample of Falder et al. (2011) has a relatively shallow 5σ limiting magnitude of 24.5 in the r -band, which has missed numerous faint objects. Fossati et al. (2021) covers a relatively small area of about 0.30 Mpc around the quasar, while a larger area needs to be investigated to study the relationship between large-scale structures and quasars. An additional complexity comes from the fact that galaxies, in particular low-mass galaxies including LAEs can be affected by photoionization effects from the strong quasar UV radiation (e.g. Kashikawa et al. 2007; Cantalupo et al. 2012). It reduces the number of galaxies in the vicinities of quasars, and thus, conceals a signal on where quasars are preferentially formed. In order to overcome these problems, it is necessary to exploit deep and wide observations of galaxies and study the environment in which quasars exist.

In this study, we present a statistical measurement of the local density environments of quasars at $z \sim 3$, by using the imaging data from Hyper Suprime-Cam Subaru Strategic Program (HSC-SSP; Aihara et al. 2018a,b, 2019, 2022) and Canada-France-Hawaii Telescope (CFHT) Large Area U-band Deep Survey (CLAUDS; Sawicki et al. 2019). The combined data allow us to construct a large sample of Lyman Break Galaxies (LBGs) at $z \sim 3$, which are less affected by the photoionization effects than are LAEs (Kashikawa et al. 2007). The overdensity map of the LBGs has been constructed from the HSC-SSP and CLAUDS data

(Toshikawa et al. 2024), in the same manner as in Toshikawa et al. (2016, 2018). We measure the overdensity significances around quasars to assess the halo mass at $z \sim 3$ (Shen et al. 2007; Eftekharzadeh et al. 2015), and interpret the results using the Extended Press Schechter model (Bond et al. 1991; Bower 1991; Lacey & Cole 1993). Possible correlations between quasar properties and their surrounding densities are also examined, which may signal the existence of the photoevaporation effect on the surrounding galaxies (Uchiyama et al. 2018).

The structure of this paper is as follows. Section 2 describes the HSC-SSP and CLAUDS data, construction of the overdensity map of LBGs, and the quasar sample taken from SDSS. We present a method to quantify the relationship between quasars and their local densities in Section 3. In Section 4, we present the results of the measured quasar environments and their possible correlation with quasar properties. In Section 5, we discuss the possible implications of the results. Finally, we present our conclusions in Section 6.

In this paper, magnitudes are given in the AB system (Oke & Gunn 1983; Fukugita et al. 1995). We adopt a Lambda cold dark matter (Λ CDM) cosmology with $H_0 = 70 \text{ km s}^{-1} \text{ Mpc}^{-1}$, $\Omega_M = 0.3$, and $\Omega_{\Lambda} = 0.7$, which are consistent with the values reported by Planck Collaboration et al. (2020). This study also uses cModel magnitude, which is measured by fitting two-component, PSF-convolved galaxy morphology model to a given object profile (Abazajian et al. 2009).

2. DATA AND SAMPLE SELECTION

2.1. HSC-SSP and CLAUDS

The HSC-SSP survey (Aihara et al. 2018a) started in 2014 and finished in 2021. It used a wide-field camera, HSC, installed on Subaru Telescope. HSC consists of 116 $2\text{K} \times 4\text{K}$ CCDs built by Hamamatsu Photonics K.K., Japan. Of these CCDs, 104 are used to obtain scientific data in a field of view of 1.5 degrees in diameter. The detailed system designs are described in Miyazaki et al. (2018) and Komiyama et al. (2018). The HSC-SSP survey consists of three layers, i.e., Wide, Deep, and Ultra-Deep, with different combinations of the area and depth of the observations. HSC-SSP provides imaging data in g, r, i, z , and y bands as well as a few narrow-band filters (Kawanomoto et al. 2018). The data were reduced by hscPipe (Bosch et al. 2018), a software developed based on the Large Synoptic Survey Telescope pipeline (Ivezic et al. 2008; Axelrod et al. 2010). The astrometric and photometric calibration are tied to the Panoramic Survey Telescope and Rapid Response System (Pan-STARRS) 1 system (Schlafly et al. 2012; Tonry et al.

2012; Magnier et al. 2013). The present work is based on the HSC-SSP Deep/UltraDeep layer data contained in the S16A internal data release which corresponds to public data release 1 (Aihara et al. 2018b).

The CLAUDS (Sawicki et al. 2019) observation provides the U -band imaging data with the CFHT/MegaCam. The U -band images are obtained with two filters, the old u^* and new u filter, because the MegaCam filter set was replaced during the survey. MegaCam consists of 40 2K×4K CCDs built by CEA Saclay, France. The CCDs cover a field of view of 1×1 square degree. The system designs are described in Boulade et al. (2003) in detail.

CLAUDS covers a large part of HSC-SSP Deep and UltraDeep layers. The u -band (u^* -band) data are available in E-COSMOS, COSMOS, DEEP2-3, and ELAIS-N1 (XMM-LSS and SXDS). The four Deep fields (E-COSMOS, XMM-LSS, ELAIS-N1, DEEP2-3) and the two UltraDeep fields (COSMOS, SXDS) cover the total area of 17.32 deg^2 with the 5σ limiting magnitudes of $(U, g, r, i, z, y)_{\text{Deep}} = (27.1, 26.8, 26.6, 26.5, 25.6, 24.8)$ and $(U, g, r, i, z, y)_{\text{UltraDeep}} = (27.7, 27.4, 27.3, 27.0, 26.4, 25.6)$ measured in 2 arcsec apertures (Aihara et al. 2018b; Sawicki et al. 2019). Sawicki et al. (2019) describes the joint processing of the CLAUDS and HSC-SSP data, which we use in the present analysis.

2.2. Overdensity map of U -dropout galaxies

We use the overdensity map of U -dropout galaxies created by Toshikawa et al. (2024). The method of constructing the map is described in detail in Toshikawa et al. (2016). We give a brief summary below.

First, U -dropout galaxies are selected from the six Deep and UltraDeep fields using the following color criteria (Sawicki et al. 2019):

For u -dropouts

$$g - r < 1.2, \quad (1)$$

$$u - g > 0.88, \quad (2)$$

$$u - g > 1.88(g - r) + 0.68, \quad (3)$$

and for u^* -dropouts

$$g - r < 1.2, \quad (4)$$

$$u^* - g > 0.9, \quad (5)$$

$$u^* - g > 1.5(g - r) + 0.75. \quad (6)$$

The typical redshift distribution of galaxies selected with these criteria is $z \sim 2.6 - 3.6$ (Toshikawa et al. 2024).

Next, the number of U -dropout galaxies is counted within an aperture distributed over the fields. The aperture size is 1.6 arcmin corresponding to 0.75 proper

Mpc (pMpc) which is the typical protocluster radius at $z \sim 3.1$ (e.g., Chiang et al. 2013; Toshikawa et al. 2016). The overdensity significance is defined as

$$\sigma = \frac{N - \bar{N}}{\sigma_N}, \quad (7)$$

where N is the number of U -dropout galaxies in the aperture. \bar{N} and σ_N represent the mean and standard deviation of the galaxy numbers measured in each of the six fields.

From the overdensity map, protocluster candidates were selected as $> 4\sigma$ overdense regions. Toshikawa et al. (2016) showed that $\sim 76 \pm 15\%$ of such candidates are expected to be real protoclusters with halo mass evolving to $> 10^{14} M_\odot$ at $z = 0$. As a result, 24 protocluster candidates were found in the present work. The completeness of finding protocluster from our overdensity map is estimated to be $\sim 5 \pm 1\%$ (Toshikawa et al. 2016).

2.3. Quasar sample

Our quasar sample is extracted from the SDSS DR16 QSO catalog (DR16Q) (Lyke et al. 2020). The catalog contains 750,414 quasars. We select the quasars whose redshift range corresponds to the redshift distribution of the U -dropout galaxies, where the selection completeness is higher than 50% (Toshikawa et al. 2016, 2024). We found 67 quasars at $z = 2.8 - 3.4$ in the Deep and UltraDeep survey fields, and visually inspected all the spectra to confirm that they are indeed quasars. Among the 67 quasars, 45 quasars are above the completeness flux limit of the eBOSS selection, and constitute the “complete sample” which will appear later. The complete limit corresponds to the eBOSS limiting magnitude of $g < 22 \text{ mag}$ or $r < 22 \text{ mag}$ (Myers et al. 2015). Assuming a quasar continuum slope of $f_\nu \propto \nu^{-0.5}$ (Vanden Berk et al. 2001) and the median C IV width of our sample $\text{FWHM} = 4300 \text{ km s}^{-1}$ (see Section 3.2.), the above completeness limit corresponds to $M_i = -25.5$ and $\log(M_{\text{BH}}/M_\odot) = 8.4$.

3. METHODS

3.1. Measurement of environment

We measure the overdensity significances in three scales. The overdensity at the exact position where a quasar is located is called the “Nearest” overdensity, hereafter. On the other hand, quasars are not always found at the center of overdense regions (Venemans et al. 2007). We thus measure the maximum overdensity significances within 1 and 3 arcmin from a quasar (hereafter “ $< 1 \text{ arcmin}$ ” and “ $< 3 \text{ arcmin}$ ”, respectively). Note that Chiang et al. (2013) found that the typical radius

of protoclusters, whose host haloes evolve to $> 10^{14}M_{\odot}$ at $z = 0$, is $\lesssim 3.0$ arcmin at $z = 3$. At this redshift, 1 and 3 arcmin corresponds to 0.47 and 1.4 pMpc, respectively. For comparison, the overdensity significances around the U -dropout galaxies themselves are also measured with the same method as for the quasars.

3.2. Measurement of quasar properties

The i -band absolute magnitudes at $z = 2$, M.I, is taken from the SDSS DR16 catalog. M.I corresponds to the rest-frame UV luminosity for objects at $z \sim 3$ (for detail, see Richards et al. 2006; Lyke et al. 2020).

Of the 67 quasars, 62 has BH mass measured and reported in SDSS DR14 catalog (Rakshit et al. 2020). We estimate the BH masses of the remaining five quasars by using the single-epoch virial BH mass estimator (e.g., Shen 2013);

$$\log\left(\frac{M_{\text{BH}}}{M_{\odot}}\right) = A + B \log\left(\frac{L}{10^{44} \text{ erg s}^{-1}}\right) + C \log\left(\frac{\Delta V}{\text{km s}^{-1}}\right), \quad (8)$$

where L [erg/s] is the quasar continuum luminosity at 1350 Å and ΔV [km s⁻¹] is the full width at half maximum (FWHM) of an emission line. For $z \sim 3$ quasars, C IV line is the common emission line to estimate the BH mass on single-epoch measurement, because the other lines do not fall into the SDSS spectral coverage. When using the above equation with C IV line, the coefficients A, B, and C are 0.660, 0.53, and 2, respectively (Vestergaard & Peterson 2006). The same procedure was also used in Rakshit et al. (2020). We subtract the best-fit continuum component from the quasar spectra with a single power law determined in the wavelength range of 1445 – 1455 Å and 1695 – 1705 Å, where no strong emission lines are present (Vestergaard & Peterson 2006). Then the C IV line width ΔV is estimated by fitting a Gaussian model.

We also measure proximity zone size with essentially the same method as described in Calverley et al. (2011). The photoionization rate of H I by quasar radiation is given by

$$\Gamma_{\text{Q}} = \int_{\nu_{\text{L}}}^{\infty} \frac{4\pi J_{\nu} \sigma_{\text{H I}}(\nu)}{h\nu} d\nu, \quad (9)$$

where ν_{L} is the frequency at the Lyman limit, J_{ν} is the intensity of quasar radiation, $\sigma_{\text{H I}}(\nu) = 6.3 \times 10^{-18} (\nu_{\text{L}}/\nu)^{2.75} \text{ cm}^2$ is the ionization cross-section of H I, and h is the Planck constant. Assuming a single power-law ($f_{\nu} \propto \nu^{-\alpha}$) for quasar radiation, equation (9) becomes

$$\Gamma_{\text{Q}} = \frac{9.5 \times 10^8 F_{\nu_{\text{L}}}}{\alpha + 2.75}, \quad (10)$$

where $F_{\nu_{\text{L}}}$ is the flux density at the Lyman limit. On the other hand, $F_{\nu_{\text{L}}}$ is expressed as

$$F_{\nu_{\text{L}}}(R) = \frac{L_{\nu_{\text{L}}}}{4\pi R^2}, \quad (11)$$

where R is the distance between the quasar and the point of interest and $L_{\nu_{\text{L}}}$ is the luminosity at the Lyman limit. Combining equation (10) and (11), we have

$$\Gamma_{\text{Q}}(R) = \frac{9.5 \times 10^8}{\alpha + 2.75} \frac{L_{\nu_{\text{L}}}}{4\pi R^2}. \quad (12)$$

Then the proximity zone size R_{pz} is defined as the distance from the quasar to the point where the ionization rate of the quasar radiation is equal to that of the background radiation, Γ_{bkg} :

$$\Gamma_{\text{Q}}(R_{\text{pz}}) = \Gamma_{\text{bkg}} \quad (13)$$

From equation (12) and (13), we obtain

$$R_{\text{pz}} = \left(\frac{9.5 \times 10^8}{4\pi(\alpha + 2.75)} \frac{L_{\nu_{\text{L}}}}{\Gamma_{\text{bkg}}} \right)^{\frac{1}{2}}. \quad (14)$$

In the estimation of the proximity zone size, the quasar continuum is fitted in the wavelength windows of 960 – 1100 Å and 1700 – 1900 Å to obtain α . We measure the average of the luminosity at 912 – 940 Å as $L_{\nu_{\text{L}}}$ and use the value of cosmic background photoionization rate $\Gamma_{\text{bkg}} = 0.792 \times 10^{-12} \text{ s}^{-1}$ at $z \sim 3$ (Haardt & Madau 2012). Figure 1 presents a clear correlation between the measured black hole masses and proximity zone sizes, both of which trace the accumulated past quasar activity. The correlation is fairly strong, with the Spearman's rank correlation coefficient and p -value of 0.69 and 5.8×10^{-10} ($\sim 6.1\sigma$), respectively. It is unlikely that selection bias due to selection effects that tend to miss more luminous quasars at a fixed black hole mass.

4. RESULTS AND DISCUSSION

Figure 2 shows the probability distributions of the overdensity significances around the quasars and the control sample of U -dropout galaxies. The distributions are similar to each other at all the three scales. The p -values of the Kolmogorov-Smirnov (KS) test between the two distributions are 0.368, 0.875, and 0.109 for the Nearest, < 1 arcmin, and < 3 arcmin cases, respectively, significantly larger than 0.05 below which the two samples are considered to be drawn from different distributions.

Figures 3 - 5 present correlations between quasar properties (UV luminosity, BH mass, and proximity zone size) and the overdensity significance, and Table 1 lists

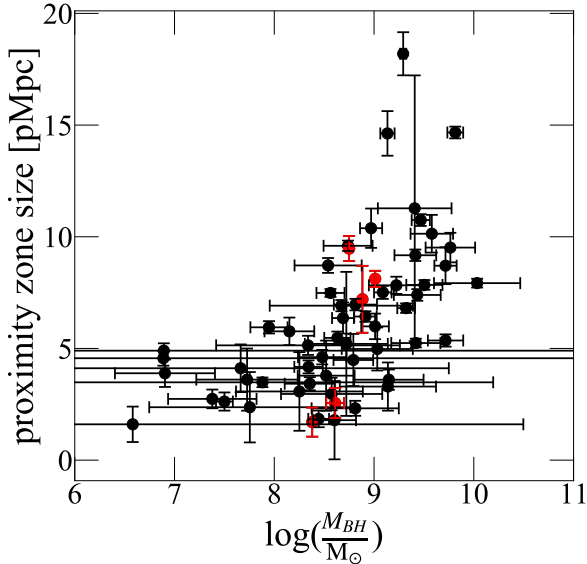


Figure 1. The relation between proximity zone sizes and the black hole masses of the 67 quasars. The black dots indicate quasars taken from the DR14 catalog of Rakshit et al. (2020), and the red dots indicate the DR16 quasar for which we measured BH masses.

the results of Spearman’s correlation tests for the all and complete samples. None of the listed properties are significantly correlated with the overdensity significance at all scales. We will discuss these results in Section 4.2.

4.1. Quasar DM halo mass

Three out of the 67 quasars were found to associate with $> 4\sigma$ overdense regions. Here we estimate the mass of the quasar dark matter haloes from this fraction using a theoretical model, and compare it with those estimated by Shen et al. (2007) and Eftekharzadeh et al. (2015). When we take into account the purity $\sim 76 \pm 15\%$ and the completeness $\sim 5 \pm 1\%$ of the protocluster candidates (Section 2.2), $(3^{+2.9}_{-1.4}) \times (0.76 \pm 0.15)/(0.05 \pm 0.01) = 46^{+44}_{-32}$ quasars are expected to be associated with protoclusters (the error comes from Poisson statistics; Gehrels 1986). Thus, $69^{+31}_{-48}\%$ of the quasars in this study are likely hosted by haloes that will evolve to $> 10^{14} M_{\odot}$ at $z = 0$. With this fraction, we estimate the halo mass at $z = 3.1$ by using the extended Press-Schechter (EPS) model (Bond et al. 1991; Bower 1991; Lacey & Cole 1993). In the EPS model, we can estimate a conditional probability $P_2(M_{t_2}, z_2 | M_{t_1}, z_1)$ that a halo mass M_{t_1} at a redshift z_1 evolves to a halo mass M_{t_2} at a later redshift z_2 (Hamana et al. 2006). Subsequently, the conditional mass function $n_2(M_{t_2}, z_2 | M_{t_1}, z_1)$ is estimated as follows

Table 1. Results of Spearman’s rank correlation tests for overdensity significance and quasar properties

UV luminosity (all sample)	ρ^*	p -value
Nearest	0.010	0.93
< 1 arcmin	-0.023	0.85
< 3 arcmin	-0.013	0.91
UV luminosity (complete sample)	ρ^*	p -value
Nearest	0.067	0.66
< 1 arcmin	-0.030	0.84
< 3 arcmin	-0.052	0.73
black hole mass (all sample)	ρ^*	p -value
Nearest	-0.24	0.052
< 1 arcmin	-0.20	0.10
< 3 arcmin	-0.19	0.13
black hole mass (complete sample)	ρ^*	p -value
Nearest	-0.23	0.12
< 1 arcmin	-0.16	0.29
< 3 arcmin	-0.15	0.34
proximity zone size	ρ^*	p -value
Nearest	-0.17	0.20
< 1 arcmin	-0.17	0.20
< 3 arcmin	-0.10	0.44

(Hamana et al. 2006):

$$n_2(M_{t_2}, z_2 | M_{t_1}, z_1) dM_{t_2} \propto \frac{1}{M_{t_2}} P_2(M_{t_2}, z_2 | M_{t_1}, z_1) dM_{t_2}. \quad (15)$$

Here, we search for possible values of M_{t_1} at $z_1 = 3.1$ that has the $69^{+31}_{-48}\%$ probability of having $M_{t_2} > 10^{14} M_{\odot}$ at $z_2 = 0$, and find that $M_{t_1} = 1.3^{+1.4}_{-0.9} \times 10^{13} h^{-1} M_{\odot}$ meets this condition. On the other hand, Shen et al. (2007) and Eftekharzadeh et al. (2015) estimated the average halo mass of about $5.0^{+3.0}_{-2.0} \times 10^{12} h^{-1} M_{\odot}$ at $z = 3.2$ and $0.66^{+0.06}_{-0.06} \times 10^{12} h^{-1} M_{\odot}$ at $z = 3.0$, respectively. Our results are therefore closer to that of Shen et al. (2007) but are also broadly consistent with Eftekharzadeh et al. (2015).

4.2. Correlation between quasar properties and local densities

In Figures 3 - 5, we found no correlation between the quasar properties and the surrounding density environments. On the other hand, Uchiyama et al. (2018) found that the UV luminosities, the BH masses, and the near zone sizes of quasars tend to correlate with the overdensity significances only at the points where quasars reside in (i.e., “Nearest” in this study) at $z \sim 4$, suggesting the photoevaporation or other forms of quasar feedback at work, but not on larger scales. Since the sample size of this study is smaller than that of Uchiyama et al. (2018),

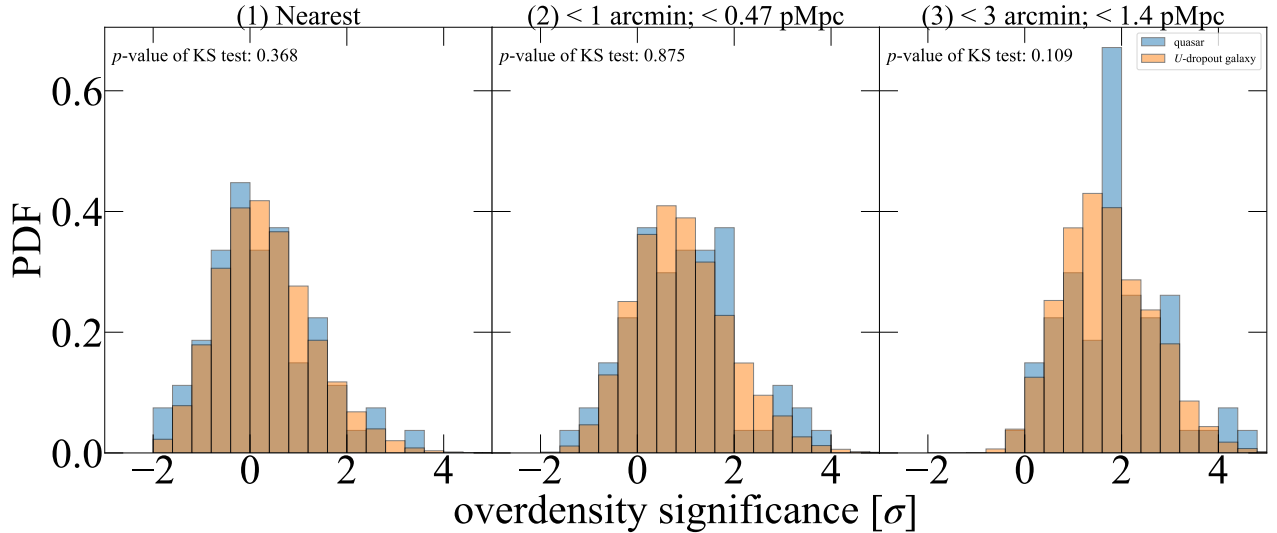


Figure 2. The probability density function (PDF) of overdensity significances around the quasars (blue bars) and around the control sample of U -dropout galaxies (orange bars). Panel (1), (2), and (3) present the cases of Nearest, < 1 arcmin, and < 3 arcmin, respectively.

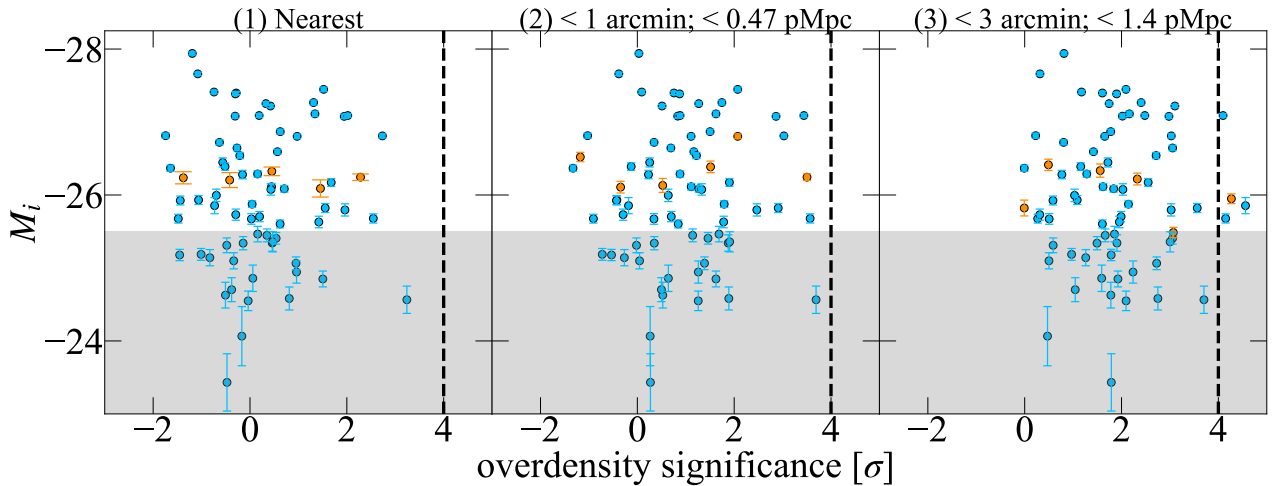


Figure 3. The quasar UV absolute magnitudes, M_i , versus the overdensity significances around the quasars. Panel (1), (2), and (3) show the cases of Nearest, < 1 arcmin, and < 3 arcmin, respectively. The median values of the complete sample in bins of the overdensity significance are indicated by the orange dots, with error bars representing the standard error of the median. The dashed vertical lines indicate the 4σ overdensity, above which the region is considered to be a protocluster. The quasar sample is not complete in the gray shaded parameter space.

it is possible that correlations are not seen even at the smallest scale.

In order to resolve such proximity effects, we plot in Figure 6 the radial density of U -dropout galaxies profiles within the projected distances of < 1.6 arcmin centered on the quasars. Here, we divide the surrounding galaxy sample into the “bright” and “faint” subsamples at the median magnitude, $r = 25.9$. The median magnitudes of the bright and faint galaxies are $r = 25.4$ and $r = 26.2$, respectively. In the left panel of Figure 6,

we find that the density of fainter galaxies decreases as they get closer to the quasar at < 1.2 arcmin. We fit two straight lines to the data points of the faint galaxies in this panel, one at < 1.2 arcmin and the other at > 1.2 arcmin. From the intersection of the two lines, we determine that 0.51 ± 0.05 pMpc ($= 1.1 \pm 0.1$ arcmin) is the distance at which the density of the faint galaxies begins to decrease toward the quasars, while the density is almost flat at the larger distances. The middle panel of Figure 6 shows that the densities of the bright galax-

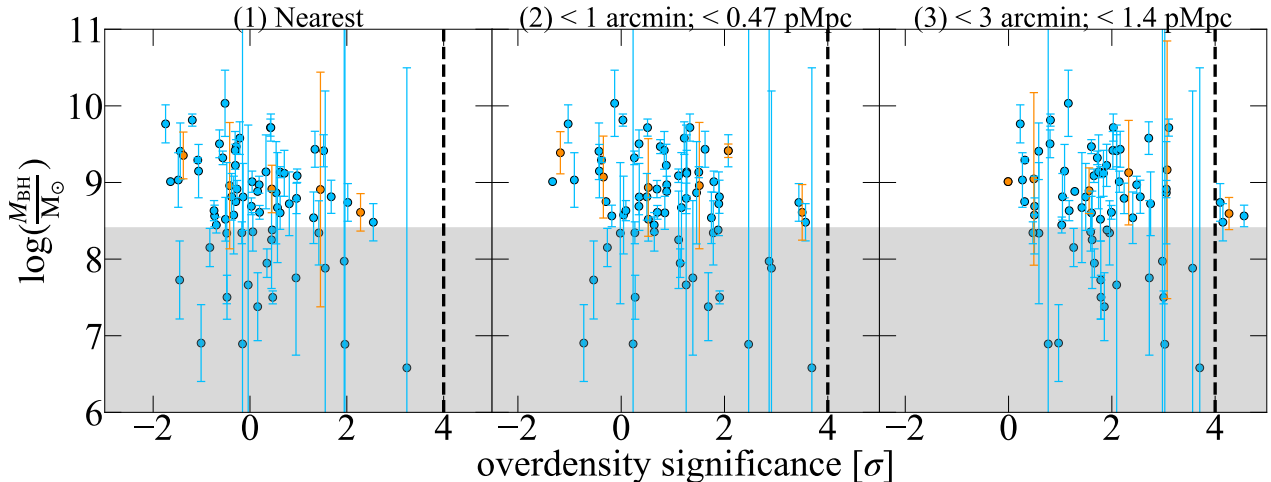


Figure 4. The quasar BH masses versus the overdensity significance. The symbols are the same as in Figure 3.

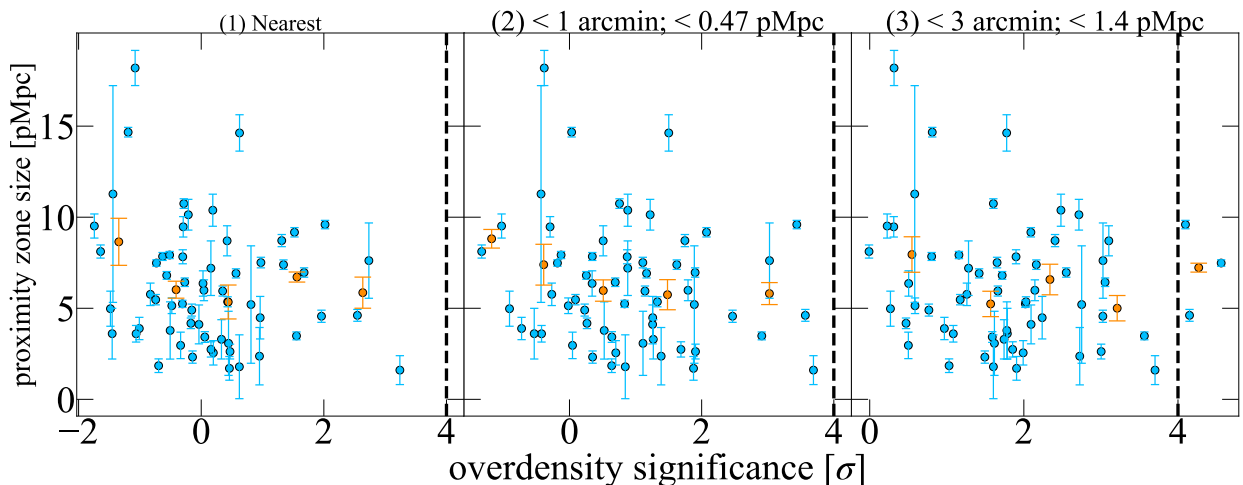


Figure 5. The proximity zone sizes versus the overdensity significance. The symbols are the same as in Figure 3.

ies around the quasars are comparable to those of the bright galaxies around the U -dropout galaxies. In the right panel, we find that the density of the faint galaxies is lower around the quasars than around the galaxies. Especially, in the vicinity of the quasars, a similar trend can be seen at the same scale as in the left panel.

We check whether this segregation of the surrounding density is caused by the photoevaporation effect by the quasar radiation. It is evaluated by comparing the UV intensity of the central quasar to the UV background radiation at the Lyman limit (e.g., Kashikawa et al. 2007; Uchiyama et al. 2019). The isotropic UV intensity J_ν from the central quasar is expressed by the following formula (Kashikawa et al. 2007; Uchiyama et al. 2019; Santos et al. 2022):

$$J_\nu = J_{21} \left(\frac{\nu}{\nu_L} \right)^\alpha \times 10^{-21} \text{ erg cm}^{-2} \text{ s}^{-1} \text{ Hz}^{-1} \text{ sr}^{-1}, \quad (16)$$

where J_{21} is the intensity at the Lyman limit. Since $J_\nu = L_\nu / (4\pi r)^2$, we have

$$r = \frac{1}{4\pi} \sqrt{\frac{L_{\nu_L}}{J_{21} (\frac{\nu}{\nu_L})^\alpha \times 10^{-21}}}. \quad (17)$$

When the intensity of quasar UV radiation J_{21} is equal to that of UV background radiation, r is equivalent to the proximity zone size. The distance $r = 0.51 \pm 0.05$ pMpc corresponds to the quasar UV intensity at the Lyman limit of $J_{21} = 27 \pm 5.4$. On the other hand, the intensity at the Lyman limit of the UV background radiation at $z = 3$ is evaluated to be $J_{21} = 1.0^{+0.5}_{-0.3}$ from the quasar proximity effect measurements (Cooke et al. 1997). Thus, it seems that the density of the faint galaxies is reduced around the quasars where the quasar UV radiation is ~ 30 times stronger than the background radiation.

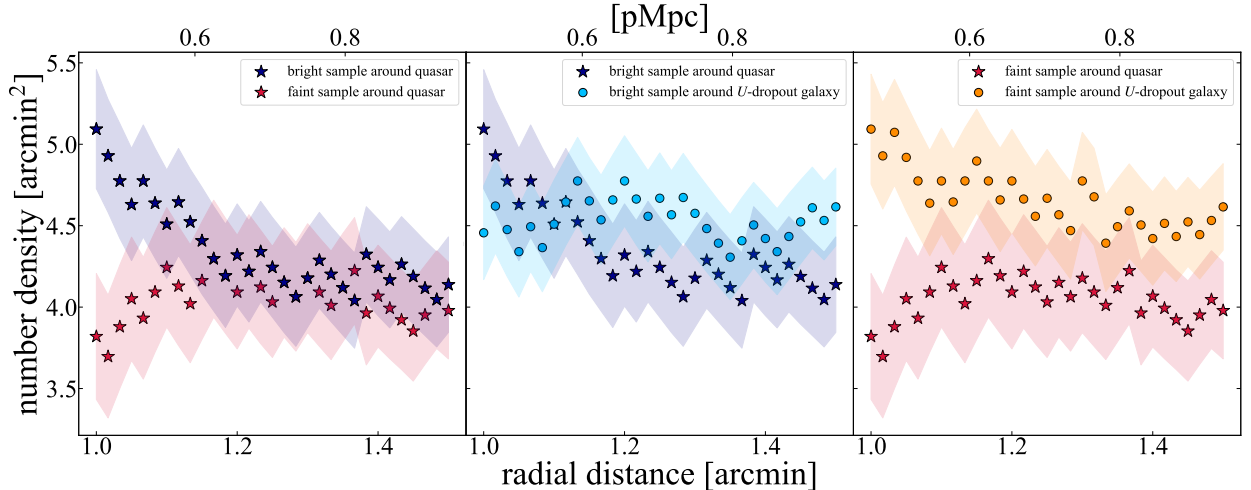


Figure 6. Radial profile of the median stacked number density of galaxies. The stars and dots represent the density of bright (blue/lightblue) and faint (red/orange) galaxies around the quasars/control sample of galaxies, respectively. The shaded regions indicate the 1σ error. Left: comparison of the density profiles of bright and faint U -dropout galaxies around quasars. Middle: comparison of the density profiles of bright U -dropout galaxies around quasars and around U -dropout galaxies. Right: comparison of the density profiles of faint U -dropout galaxies around quasars and around U -dropout galaxies.

Harikane et al. (2022) estimated the halo mass of U -dropout galaxies, in essentially the same luminosity range as our U -dropout galaxies, to be $\sim 2.2 \times 10^{11} M_{\odot}$. Kashikawa et al. (2007) suggests that quasar radiation at Lyman limit of $J_{21} = 30$ can suppress star formation in a halo with a virial mass of $M_{\text{vir}} < 10^{10} M_{\odot}$, but the halo mass of our sample is significantly larger. Santos et al. (2022) found a similar result in the case of LAE environments. The brighter LAEs prefer to reside in more massive DM haloes and should be expected to be in denser regions but they reported the opposite trend, with fainter LAEs avoiding the bright central LAEs. This may imply that UV radiation from the central LAEs inhibits the formation of surrounding LAEs. They estimated the J_{21} of the central LAEs and compared the mass of the surrounding halo with the virial mass at which star formation is suppressed, based on Kashikawa et al. (2007). While they found that the UV radiation of central LAEs can suppress the star formation at $M_{\text{vir}} < 10^9 M_{\odot}$, the average halo mass of the LAEs is $M_{\text{vir}} \sim 10^{10-11} M_{\odot}$ measured by clustering analysis in Ouchi et al. (2018), indicating that star formation can be suppressed at such larger haloes. Galaxies in a massive halo may thus be affected by photoevaporation, depending on the central UV radiation and property of the surrounding galaxies.

5. CONCLUSION

We have measured the local density environments around SDSS luminous quasars at $z \sim 3$ using the imaging data from HSC-SSP and CLAUDS. We measured the U -dropout galaxy densities around 67 quasars, and

found that the density distributions of the quasars and the U -dropout galaxies are comparable. Three quasars are associated with protocluster candidates within a separation of 3 arcmin. The fraction of such association suggests that quasars at this epoch occupy haloes with a mass of $1.3_{-0.9}^{+1.4} \times 10^{13} h^{-1} M_{\odot}$, which is consistent with a measurement by Shen et al. (2007). We also analyzed the correlation between the surrounding densities and quasar properties (UV luminosity, BH mass, and proximity zone size). As a result, no significant correlations are found. Finally, we examined the radial density profile of galaxies around the quasars. The local density of faint U -dropout galaxies are found to be significantly lower than that of bright U -dropout galaxies within a projected distance of 0.51 ± 0.05 pMpc from the quasars. This distance corresponds the quasar UV intensity at the Lyman limit of $J_{21} = 27 \pm 5.4$, which is about 30 times that of the background radiation. Photoevaporation may suppress galaxy formation at short distances where the quasar UV intensity is strong, even in massive haloes.

ACKNOWLEDGMENTS

Y.S. was supported by JST, the establishment of university fellowships towards the creation of science technology innovation, Grant Number JPMJFS2131 and JST SPRING, Japan Grant Number JPMJSP2162. Y.M. was supported by the Japan Society for the Promotion of Science (JSPS) KAKENHI grant No. 21H04494. C.L. acknowledges support from the National Natural Science Foundation of China (NSFC, Grant No. 11933003), 111 project (No. B20019), and Key Labora-

tory for Particle Physics, Astrophysics and Cosmology, Ministry of Education.

The Hyper Suprime-Cam (HSC) collaboration includes the astronomical communities of Japan and Taiwan, and Princeton University. The HSC instrumentation and software were developed by the National Astronomical Observatory of Japan (NAOJ), the Kavli Institute for the Physics and Mathematics of the Universe (Kavli IPMU), the University of Tokyo, the High Energy Accelerator Research Organization (KEK), the Academia Sinica Institute for Astronomy and Astrophysics in Taiwan (ASIAA), and Princeton University. Funding was contributed by the FIRST program from Japanese Cabinet Office, the Ministry of Education, Culture, Sports, Science and Technology (MEXT), the Japan Society for the Promotion of Science (JSPS), Japan Science and Technology Agency (JST), the Toray Science Foundation, NAOJ, Kavli IPMU, KEK, ASIAA, and Princeton University. This paper makes use of software developed for the Large Synoptic Survey Telescope. We thank the LSST Project for making their code available as free software at <http://dm.lsst.org> The Pan-STARRS1 Surveys (PS1) have been made possible through contributions of the Institute for Astronomy, the University of Hawaii, the Pan-STARRS Project Office, the Max-Planck Society and its participating institutes, the Max Planck Institute for Astronomy, Heidelberg and the Max Planck Institute for Extraterrestrial Physics, Garching, The Johns Hopkins University, Durham University, the University of Edinburgh, Queen's University Belfast, the Harvard-Smithsonian Center for Astrophysics, the Las Cumbres Observatory Global Telescope Network Incorporated, the National Central University of Taiwan, the Space Telescope Sci-

ence Institute, the National Aeronautics and Space Administration under Grant No. NNX08AR22G issued through the Planetary Science Division of the NASA Science Mission Directorate, the National Science Foundation under Grant No. AST-1238877, the University of Maryland, and Eotvos Lorand University (ELTE) and the Los Alamos National Laboratory. Based on data collected at the Subaru Telescope and retrieved from the HSC data archive system, which is operated by Subaru Telescope and Astronomy Data Center at National Astronomical Observatory of Japan. This work is based on data collected at the Subaru Telescope and retrieved from the HSC data archive system, which is operated by the Subaru Telescope and Astronomy Data Center at the National Astronomical Observatory of Japan.

These data were obtained and processed as part of the CFHT Large Area U-band Deep Survey (CLAUDS), which is a collaboration between astronomers from Canada, France, and China described in [Sawicki et al. \(2019\)](#). CLAUDS is based on observations obtained with MegaPrime/ MegaCam, a joint project of CFHT and CEA/DAPNIA, at the CFHT which is operated by the National Research Council (NRC) of Canada, the Institut National des Science de l'Univers of the Centre National de la Recherche Scientifique (CNRS) of France, and the University of Hawaii. CLAUDS uses data obtained in part through the Telescope Access Program (TAP), which has been funded by the National Astronomical Observatories, Chinese Academy of Sciences, and the Special Fund for Astronomy from the Ministry of Finance of China. CLAUDS uses data products from TERAPIX and the Canadian Astronomy Data Centre (CADC) and was carried out using resources from Compute Canada and Canadian Advanced Network For Astrophysical Research (CANFAR).

REFERENCES

- Abazajian, K. N., Adelman-McCarthy, J. K., Agüeros, M. A., et al. 2009, *ApJS*, 182, 543, doi: [10.1088/0067-0049/182/2/543](https://doi.org/10.1088/0067-0049/182/2/543)
- Aihara, H., Arimoto, N., Armstrong, R., et al. 2018a, *PASJ*, 70, S4, doi: [10.1093/pasj/psx066](https://doi.org/10.1093/pasj/psx066)
- Aihara, H., Armstrong, R., Bickerton, S., et al. 2018b, *PASJ*, 70, S8, doi: [10.1093/pasj/psx081](https://doi.org/10.1093/pasj/psx081)
- Aihara, H., AlSayyad, Y., Ando, M., et al. 2019, *PASJ*, 71, 114, doi: [10.1093/pasj/psz103](https://doi.org/10.1093/pasj/psz103)
- . 2022, *PASJ*, 74, 247, doi: [10.1093/pasj/psab122](https://doi.org/10.1093/pasj/psab122)
- Axelrod, T., Kantor, J., Lupton, R. H., & Pierfederici, F. 2010, *Proc. SPIE*
- Bacon, R., Accardo, M., Adjali, L., et al. 2010, in *Society of Photo-Optical Instrumentation Engineers (SPIE) Conference Series*, Vol. 7735, *Ground-based and Airborne Instrumentation for Astronomy III*, ed. I. S. McLean, S. K. Ramsay, & H. Takami, 773508, doi: [10.1117/12.856027](https://doi.org/10.1117/12.856027)
- Benson, A. J., Frenk, C. S., Lacey, C. G., Baugh, C. M., & Cole, S. 2002, *MNRAS*, 333, 177, doi: [10.1046/j.1365-8711.2002.05388.x](https://doi.org/10.1046/j.1365-8711.2002.05388.x)
- Bond, J. R., Cole, S., Efsthathiou, G., & Kaiser, N. 1991, *ApJ*, 379, 440, doi: [10.1086/170520](https://doi.org/10.1086/170520)
- Bosch, J., Armstrong, R., Bickerton, S., et al. 2018, *PASJ*, 70, S5, doi: [10.1093/pasj/psx080](https://doi.org/10.1093/pasj/psx080)

- Boulade, O., Charlot, X., Abbon, P., et al. 2003, in Society of Photo-Optical Instrumentation Engineers (SPIE) Conference Series, Vol. 4841, Instrument Design and Performance for Optical/Infrared Ground-based Telescopes, ed. M. Iye & A. F. M. Moorwood, 72–81, doi: [10.1117/12.459890](https://doi.org/10.1117/12.459890)
- Bower, R. G. 1991, MNRAS, 248, 332, doi: [10.1093/mnras/248.2.332](https://doi.org/10.1093/mnras/248.2.332)
- Calverley, A. P., Becker, G. D., Haehnelt, M. G., & Bolton, J. S. 2011, MNRAS, 412, 2543, doi: [10.1111/j.1365-2966.2010.18072.x](https://doi.org/10.1111/j.1365-2966.2010.18072.x)
- Cantalupo, S., Lilly, S. J., & Haehnelt, M. G. 2012, MNRAS, 425, 1992, doi: [10.1111/j.1365-2966.2012.21529.x](https://doi.org/10.1111/j.1365-2966.2012.21529.x)
- Chiang, Y.-K., Overzier, R., & Gebhardt, K. 2013, ApJ, 779, 127, doi: [10.1088/0004-637X/779/2/127](https://doi.org/10.1088/0004-637X/779/2/127)
- Cooke, A. J., Espey, B., & Carswell, R. F. 1997, MNRAS, 284, 552, doi: [10.1093/mnras/284.3.552](https://doi.org/10.1093/mnras/284.3.552)
- Dawson, K. S., Schlegel, D. J., Ahn, C. P., et al. 2013, AJ, 145, 10, doi: [10.1088/0004-6256/145/1/10](https://doi.org/10.1088/0004-6256/145/1/10)
- Eftekharzadeh, S., Myers, A. D., White, M., et al. 2015, MNRAS, 453, 2779, doi: [10.1093/mnras/stv1763](https://doi.org/10.1093/mnras/stv1763)
- Falder, J. T., Stevens, J. A., Jarvis, M. J., et al. 2011, ApJ, 735, 123, doi: [10.1088/0004-637X/735/2/123](https://doi.org/10.1088/0004-637X/735/2/123)
- Fanidakis, N., Macciò, A. V., Baugh, C. M., Lacey, C. G., & Frenk, C. S. 2013, MNRAS, 436, 315, doi: [10.1093/mnras/stt1567](https://doi.org/10.1093/mnras/stt1567)
- Fazio, G. G., Hora, J. L., Allen, L. E., et al. 2004, ApJS, 154, 10, doi: [10.1086/422843](https://doi.org/10.1086/422843)
- Font-Ribera, A., Arnau, E., Miralda-Escudé, J., et al. 2013, JCAP, 2013, 018, doi: [10.1088/1475-7516/2013/05/018](https://doi.org/10.1088/1475-7516/2013/05/018)
- Fossati, M., Fumagalli, M., Lofthouse, E. K., et al. 2021, MNRAS, 503, 3044, doi: [10.1093/mnras/stab660](https://doi.org/10.1093/mnras/stab660)
- Fukugita, M., Shimasaku, K., & Ichikawa, T. 1995, PASP, 107, 945, doi: [10.1086/133643](https://doi.org/10.1086/133643)
- Gehrels, N. 1986, ApJ, 303, 336, doi: [10.1086/164079](https://doi.org/10.1086/164079)
- Haardt, F., & Madau, P. 2012, ApJ, 746, 125, doi: [10.1088/0004-637X/746/2/125](https://doi.org/10.1088/0004-637X/746/2/125)
- Hamana, T., Yamada, T., Ouchi, M., Iwata, I., & Kodama, T. 2006, MNRAS, 369, 1929, doi: [10.1111/j.1365-2966.2006.10472.x](https://doi.org/10.1111/j.1365-2966.2006.10472.x)
- Harikane, Y., Ono, Y., Ouchi, M., et al. 2022, ApJS, 259, 20, doi: [10.3847/1538-4365/ac3dfc](https://doi.org/10.3847/1538-4365/ac3dfc)
- Ivezic, Z., Axelrod, T., Brandt, W. N., et al. 2008, Serbian Astron. J., 176, 1, doi: [10.2298/SAJ0876001I](https://doi.org/10.2298/SAJ0876001I)
- Kashikawa, N., Kitayama, T., Doi, M., et al. 2007, ApJ, 663, 765, doi: [10.1086/518410](https://doi.org/10.1086/518410)
- Kawanomoto, S., Uruguchi, F., Komiyama, Y., et al. 2018, PASJ, 70, 66, doi: [10.1093/pasj/psy056](https://doi.org/10.1093/pasj/psy056)
- Kikuta, S., Imanishi, M., Matsuoka, Y., et al. 2017, ApJ, 841, 128, doi: [10.3847/1538-4357/aa72f0](https://doi.org/10.3847/1538-4357/aa72f0)
- Komiyama, Y., Obuchi, Y., Nakaya, H., et al. 2018, PASJ, 70, S2, doi: [10.1093/pasj/psx069](https://doi.org/10.1093/pasj/psx069)
- Lacey, C., & Cole, S. 1993, MNRAS, 262, 627, doi: [10.1093/mnras/262.3.627](https://doi.org/10.1093/mnras/262.3.627)
- Lyke, B. W., Higley, A. N., McLane, J. N., et al. 2020, ApJS, 250, 8, doi: [10.3847/1538-4365/aba623](https://doi.org/10.3847/1538-4365/aba623)
- Magnier, E. A., Schlafly, E., Finkbeiner, D., et al. 2013, ApJS, 205, 20, doi: [10.1088/0067-0049/205/2/20](https://doi.org/10.1088/0067-0049/205/2/20)
- Miyazaki, S., Komiyama, Y., Kawanomoto, S., et al. 2018, PASJ, 70, S1, doi: [10.1093/pasj/psx063](https://doi.org/10.1093/pasj/psx063)
- Myers, A. D., Brunner, R. J., Richards, G. T., et al. 2006, ApJ, 638, 622, doi: [10.1086/499093](https://doi.org/10.1086/499093)
- Myers, A. D., Palanque-Delabrouille, N., Prakash, A., et al. 2015, ApJS, 221, 27, doi: [10.1088/0067-0049/221/2/27](https://doi.org/10.1088/0067-0049/221/2/27)
- Oke, J. B., & Gunn, J. E. 1983, ApJ, 266, 713, doi: [10.1086/160817](https://doi.org/10.1086/160817)
- Ouchi, M., Harikane, Y., Shibuya, T., et al. 2018, PASJ, 70, S13, doi: [10.1093/pasj/psx074](https://doi.org/10.1093/pasj/psx074)
- Planck Collaboration, Aghanim, N., Akrami, Y., et al. 2020, A&A, 641, A6, doi: [10.1051/0004-6361/201833910](https://doi.org/10.1051/0004-6361/201833910)
- Rakshit, S., Stalin, C. S., & Kotilainen, J. 2020, ApJS, 249, 17, doi: [10.3847/1538-4365/ab99c5](https://doi.org/10.3847/1538-4365/ab99c5)
- Richards, G. T., Strauss, M. A., Fan, X., et al. 2006, AJ, 131, 2766, doi: [10.1086/503559](https://doi.org/10.1086/503559)
- Ross, N. P., Shen, Y., Strauss, M. A., et al. 2009, ApJ, 697, 1634, doi: [10.1088/0004-637X/697/2/1634](https://doi.org/10.1088/0004-637X/697/2/1634)
- Santos, D. J. D., Goto, T., Hashimoto, T., et al. 2022, MNRAS, 516, 5601, doi: [10.1093/mnras/stac2541](https://doi.org/10.1093/mnras/stac2541)
- Sawicki, M., Arnouts, S., Huang, J., et al. 2019, MNRAS, 489, 5202, doi: [10.1093/mnras/stz2522](https://doi.org/10.1093/mnras/stz2522)
- Schlafly, E. F., Finkbeiner, D. P., Jurić, M., et al. 2012, ApJ, 756, 158, doi: [10.1088/0004-637X/756/2/158](https://doi.org/10.1088/0004-637X/756/2/158)
- Shen, Y. 2013, BASI, 41, 61, <https://arxiv.org/abs/1302.2643>
- Shen, Y., Strauss, M. A., Oguri, M., et al. 2007, AJ, 133, 2222, doi: [10.1086/513517](https://doi.org/10.1086/513517)
- Simpson, C., Mortlock, D., Warren, S., et al. 2014, MNRAS, 442, 3454, doi: [10.1093/mnras/stu1116](https://doi.org/10.1093/mnras/stu1116)
- Tonry, J. L., Stubbs, C. W., Lykke, K. R., et al. 2012, ApJ, 750, 99, doi: [10.1088/0004-637X/750/2/99](https://doi.org/10.1088/0004-637X/750/2/99)
- Toshikawa, J., Kashikawa, N., Overzier, R., et al. 2016, ApJ, 826, 114, doi: [10.3847/0004-637X/826/2/114](https://doi.org/10.3847/0004-637X/826/2/114)
- Toshikawa, J., Uchiyama, H., Kashikawa, N., et al. 2018, PASJ, 70, S12, doi: [10.1093/pasj/psx102](https://doi.org/10.1093/pasj/psx102)
- Toshikawa, J., Wuyts, S., Kashikawa, N., et al. 2024, MNRAS, 527, 6276, doi: [10.1093/mnras/stad3162](https://doi.org/10.1093/mnras/stad3162)
- Uchiyama, H., Toshikawa, J., Kashikawa, N., et al. 2018, PASJ, 70, S32, doi: [10.1093/pasj/psx112](https://doi.org/10.1093/pasj/psx112)

- Uchiyama, H., Kashikawa, N., Overzier, R., et al. 2019, ApJ, 870, 45, doi: [10.3847/1538-4357/aaef7b](https://doi.org/10.3847/1538-4357/aaef7b)
- Utsumi, Y., Goto, T., Kashikawa, N., et al. 2010, ApJ, 721, 1680, doi: [10.1088/0004-637X/721/2/1680](https://doi.org/10.1088/0004-637X/721/2/1680)
- Vanden Berk, D. E., Richards, G. T., Bauer, A., et al. 2001, AJ, 122, 549, doi: [10.1086/321167](https://doi.org/10.1086/321167)
- Venemans, B. P., Röttgering, H. J. A., Miley, G. K., et al. 2007, A&A, 461, 823, doi: [10.1051/0004-6361:20053941](https://doi.org/10.1051/0004-6361:20053941)
- Vestergaard, M., & Peterson, B. M. 2006, ApJ, 641, 689, doi: [10.1086/500572](https://doi.org/10.1086/500572)
- White, M., Myers, A. D., Ross, N. P., et al. 2012, MNRAS, 424, 933, doi: [10.1111/j.1365-2966.2012.21251.x](https://doi.org/10.1111/j.1365-2966.2012.21251.x)
- York, D. G., Adelman, J., Anderson, John E., J., et al. 2000, AJ, 120, 1579, doi: [10.1086/301513](https://doi.org/10.1086/301513)